IEEE Access
Multidisciplinary | Rapid Review | Open Access Journal

Received December 19, 2019, accepted January 17, 2020, date of publication January 30, 2020, date of current version February 6, 2020.

Digital Object Identifier 10.1109/ACCESS.2020.2970440

Classification and Spectral Mapping of Stationary and Moving Objects in Road Environments Using FMCW Radar

HEEMANG SONG AND HYUN-CHOOL SHIN, (Member, IEEE)
Department of Electronic Engineering, Soongsil University, Seoul 156-743, South Korea

Corresponding author: Hyun-Chool Shin (shinhc@ssu.ac.kr)

This work was supported by the Starting growth Technological Research and Development Program funded by the Small and Medium Business Administration (SMBA), South Korea under Grant S2791295.

ABSTRACT In order to establish a reliable map of the road environment, this paper aims to classify the stationary and moving objects unlike the previous researches which generally focus on object recognition. The characteristics of the radar signals of stationary and moving objects were analyzed and the relation between the slope of pattern in radar time-frequency spectrum and relative velocity of the object was described mathematically. To discriminate the stationary and moving objects, the difference between the measured velocity by the slope and the velocity of the ego-vehicle was proposed as a feature. The statistical characteristics of stationary and moving objects according to the proposed feature were modeled using Gaussian model. To investigate the performance of the proposed method, the similarity between modeling of stationary and moving objects was quantified. Additionally, the receiver operating characteristics (ROC) curve and the correlation coefficient between the proposed feature and the ground-truth feature map was applied to verify the performance.

INDEX TERMS Automotive radar, radar signal processing, road environment map, FMCW radar, object classification.

I. INTRODUCTION

As recent advanced automobile technology develops, autonomous vehicles are becoming a reality and a hot topic in the automobile market [1]. In order to achieve more accurate and perfect autonomous driving, it is essential to establish a reliable map of the road environment surrounding the vehicle [2], [3]. As a result, various studies of constructing a map for autonomous driving have been conducted. In the case of the research conducted in the 2007 DARPA Urban Challenge [4] and in the case of the road boundary and object recognition research [5], the maps were mainly constructed using the camera and lidar sensors [6]. However, because the camera and lidar sensors are sensitive to visibility and weather conditions, the radar sensor that is robust to these conditions is attracting attention [7], [8]. In addition, Bosch recently announced at TU-Automotive Detroit 2017 that it will create a radar road signature that builds a high-resolution map by determining the relative position of all objects such as guard rails and road signs using radar sensors.

Road map construction should precede the recognition of various objects in the road environment. So, various studies have been conducted to recognize objects using radar. There have been researches on road recognition using tracking and probability hypothesis density filter [2], [3], road structure recognition based on statistical characteristic [9], road marking analysis for road line recognition [8], forward bridge identification using frequency analysis of received radar signals [10], and radar signal analysis for pedestrian [11] and bicycle user recognition [12]. Most studies use the frequency modulated continuous wave (FMCW) radar, which performs object recognition by measuring the beat frequencies in the frequency domain [13]. Recently, studies have been conducted in the time-frequency domain, instead of the frequency domain. There has been research on the recognition of iron tunnels by measuring the degree of spectral spreading through the analysis of the spectrum characteristics of the received radar signal in iron tunnel [14], and

The associate editor coordinating the review of this manuscript and approving it for publication was Weimin Huang.

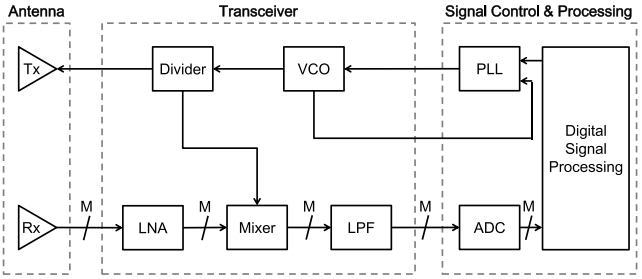

FIGURE 1. FMCW radar system structure.

harmonic clutter suppression by measuring the periodicity of harmonic clutters using spectrum [15], [16]. In this paper, for supporting the construction of the road map containing various objects, we focus on stationary and moving object classification.

This paper analyzes the characteristics of the radar signals of stationary and moving objects, and maps stationary and moving objects to the time-frequency spectrum. The beat frequency, which is the frequency difference between the transmitted and the received signal, changes according to the movement and distance of the object. The characteristics of the stationary and moving objects are compared by analyzing the beat frequency in the time-frequency spectrum. In the time-frequency spectrum, various patterns are analyzed according to the movement of the object. This paper confirmed that the slope of this pattern is related to the relative velocity, measured it using the Hough transform [17], and converted it to a velocity. In addition, the statistical characteristics defined as the difference between the measured velocity by the slope and the velocity of the ego-vehicle is modeled. Hellinger distance [18] and KS-test [19] are used to quantify the accuracy of statistical modeling. As a result, the stationary and moving objects are mapped on the time-frequency spectrum, and the performance of the proposed method is verified through the ROC curve [20] and correlation [21] with the ground-truth feature map.

The rest of this paper is organized as follows. The FMCW radar system and radar signal model are introduced in Section II. In Section III, the analysis of the spectral characteristics of the received signal in accordance with stationary and moving objects is explained. Section IV comprises of the detailed explanation of the proposed method which detects the slope in the time-frequency spectrum. Then, the experimental results of classifying the stationary and moving objects are provided in Section V. Finally, we summarize and conclude our work in Section VI.

II. RADAR MODEL

In this paper, we have used a 77 GHz FMCW radar. Fig. 1 shows the structure of the FMCW radar that consists of an antenna module, transceiver unit, and signal control and processing unit. The antenna module converts electrical radio-frequency (RF) signal into electromagnetic wave, while the transceiver unit generates the RF signal and processes the received RF signal. The signal control and processing unit handles the schedule of FMCW modulation and radar scanning. The transmission channel is a single channel, and the receiving channel consists of K uniform linear arrays. A scan is the time that includes transmission, reception, and signal processing, and the duration period of a single scan is 50 ms. In each scan, identical signals are transmitted. If the signal transmitted from the FMCW radar is reflected by L objects, the received signal in the kth array is expressed as follows [22], [23]:

$$r_k(t) = \sum_{i=0}^{L-1} A_k(i) \cos\left(2\pi f(i)t + \phi_k(i)\right) \tag{1}$$

where $A_k(i)$ is the amplitude of the signal reflected from each object at the kth array antenna; $\phi_k(i)$ is the phase of the each received signal; and $f(i)$ is the beat frequency, which is the frequency difference between the transmitted signal and the received signal, and is composed of $f_r(i)$ (which is the frequency difference according to the distance of an object) and $f_d(i)$ (which is the frequency difference due to the relative velocity between the radar and each object). $f(i)$, $f_r(i)$, and $f_d(i)$ are as follows:

$$\begin{aligned} Rclf(i) &= f_r(i) - f_d(i) \quad \text{in up-chirp duration} \\ &= f_r(i) + f_d(i) \quad \text{in down-chirp duration} \end{aligned} \tag{2}$$

$$f_r(i) = \frac{2B}{cT} R(i) \tag{3}$$

$$f_d(i) = \frac{2f_c}{c} V_r(i) \tag{4}$$

where, B is the bandwidth; T is the chirp duration; c is the speed of light; f_c refers to the center frequency; $R(i)$ and $V_r(i)$ are the distance and relative velocity between the radar and each object, respectively; and $r_k(n)$ is the discrete-time signal of $r_k(t)$, which is as follows:

$$r_k(n) = \sum_{i=0}^{L-1} A_k(i) \cos\left(2\pi f(i) n T_s + \phi_k(i)\right) \tag{5}$$

where, $n (0 \le n < N)$ is the discrete-time index of the received signal during a single scan; N is the total number of samples in a single scan; and T_s represents the sampling time.

If these received signals are transformed using the short-time Fourier transform (STFT), they are as follows:

$$R_k(f, m) = \sum_{n=0}^{N-1} r_k(n + (m-1)N) e^{-j\frac{2\pi f}{N} n} \tag{6}$$

where, f is the frequency index; and m is the scan index. The window length is 2048 and block window is used. Using (6), the magnitude response in the frequency domain is as follows:

$$P(f, m) = \left| \sum_{k=0}^{K-1} R_k(f, m) \right| \tag{7}$$

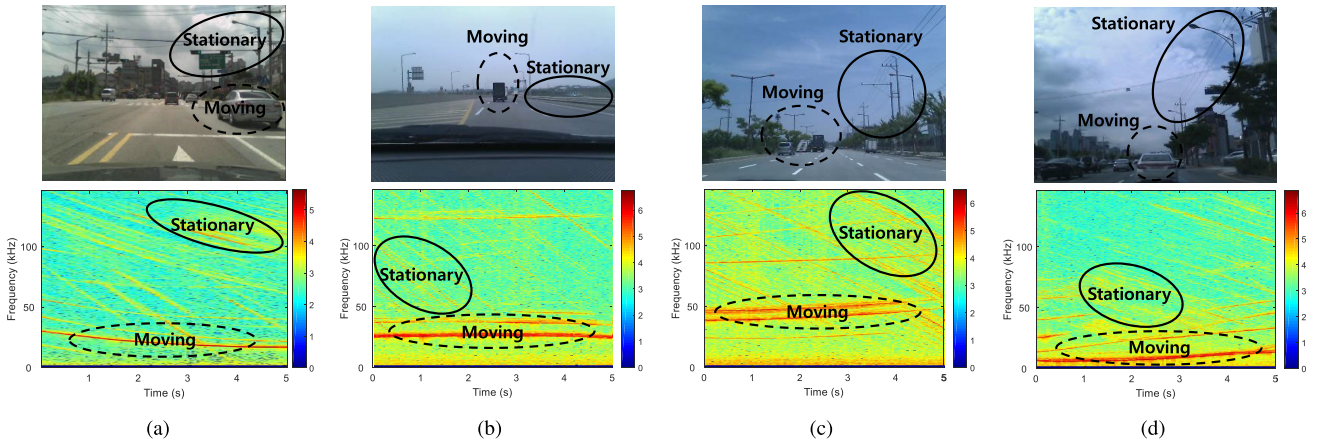

FIGURE 2. Time-frequency representation of the received radar signal in dB scale under normal road condition. (a) road sign, (b) guardrail, (c) far streetlight, and (d) near streetlight.

III. SPECTRAL CHARACTERISTICS OF OBJECTS

In order to understand the radar signal characteristics of stationary and moving objects, the time-frequency spectrum was analyzed using the signal acquired at a normal road. Fig. 2 shows the magnitude response using the STFT of the received signal under normal road, and represents the change of the beat frequency over time of each object. As the beat frequency changes according to the velocity and distance of the object, various slopes appear on the time-frequency spectrum in Fig. 2. Fig. 2(a) shows that the stationary object that is a road sign reveals a decreasing frequency over time in the high-frequency band. Although the frequency of the forward moving object is also decreased, the frequency reduction of the moving object is smaller than that of the stationary object. Fig. 2(b) shows the stationary object that is a guardrail reveals a constantly decreasing frequency, while the moving object shows a zero slope with no frequency change over time. Fig. 2(c) and (d) show the stationary object that is a streetlight shows a decreasing frequency in the time-frequency spectrum, and the frequency of the moving object is slightly increasing. Fig. 2 shows that the stationary objects have a decreasing frequency over time, while the forward moving object shows a relatively small decreasing slope or an increasing slope, according to the velocity of the object.

In order to understand the meaning of the slope in the time-frequency spectrum, the slope of the ith object is defined as:

$$s(i) = \frac{\Delta f(i)}{\Delta t} = \frac{\Delta f_r(i) \pm \Delta f_d(i)}{\Delta t} \tag{8}$$

The slope $s(i)$ is the frequency variation over time, and is represented as an equation that is composed of $f_r(i)$ and $f_d(i)$ according to (2). Using (3) and (4), the slope $s(i)$ can be expressed as follows:

$$s(i) = \frac{2B}{cT}\frac{\Delta R(i)}{\Delta t} \pm \frac{2f_c}{c}\frac{\Delta V_r(i)}{\Delta t} \tag{9}$$

The first term in (9) is the variation in distance over time, which is related to the relative velocity of the object. The second term is the variation in relative velocity over time, which refers to the curvature of the slope in the time-frequency spectrum. Assuming that the variation of the velocity ΔV_r during Δt is small ($\frac{\Delta V_r}{\Delta t} \cong 0$), the curvature characteristics of the slope can be ignored. So the slope $s(i)$ is approximated as follows:

$$s(i) \approx \frac{2B}{cT}\frac{\Delta R(i)}{\Delta t} = \frac{2B}{cT}V_r(i) \tag{10}$$

Since B, T and c are constants in (10), the slope in the time-frequency spectrum is proportional to the relative velocity ($V_r(i)$) of the object. When the ith object is a stationary object, the relative velocity $V_r(i)$ has the following relationship with the velocity of the ego-vehicle:

$$V_r(i) = -V_{ego} \tag{11}$$

Then, the slope $s(i)$ of the stationary object in the time-frequency spectrum has the following relationship:

$$s(i) \propto -V_{ego} \tag{12}$$

Thus, if we measure the slope in the time-frequency spectrum, we can discriminate stationary and moving objects.

IV. SLOPE DETECTION IN THE TIME-FREQUENCY SPECTRUM

The Hough transform is the most commonly used method for detecting the slope. This technique changes the coordinates in space (x, y) to coordinates in the Hough space (θ, ρ). The relation between x, y, θ, and ρ is expressed by the following (13):

$$\rho = x\cos\theta + y\sin\theta \tag{13}$$

where ρ is the vertical distance from the origin to the straight line, and θ is the angle between the x axis and the vertical line connecting the origin with the straight line. Fig. 3 shows the time-frequency spectrums and the road images under normal road condition. Fig. 3(a) and (b) show that there is a stationary vehicle to the front right, and a moving vehicle to the far front left.

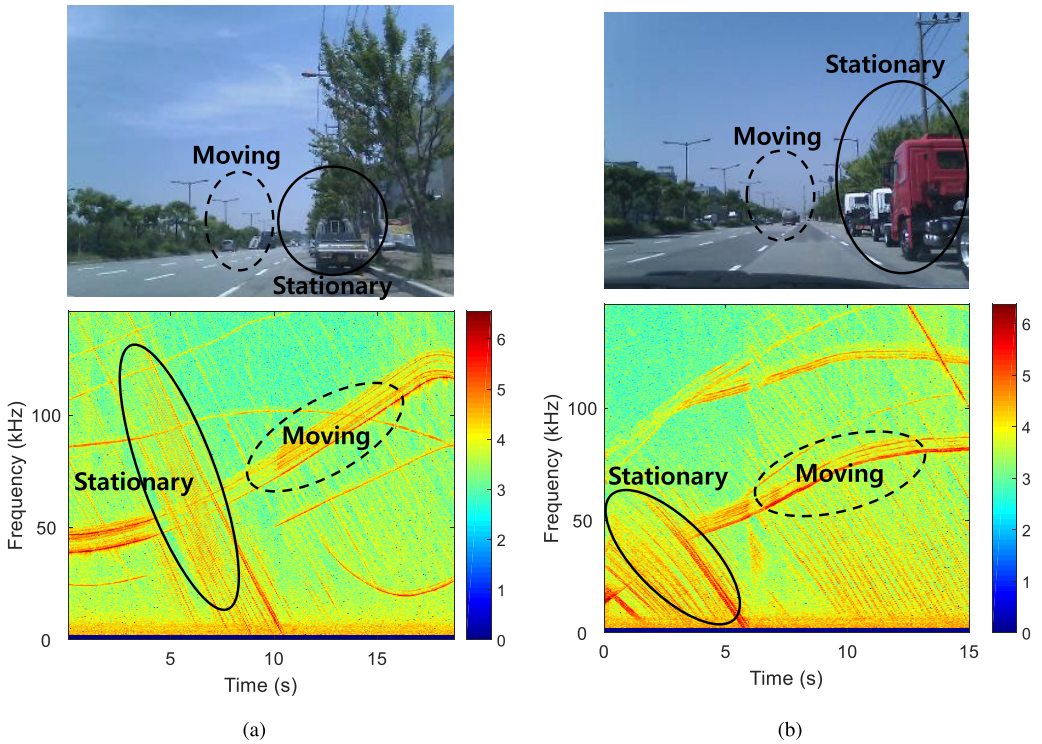

FIGURE 3. Time-frequency representation in dB scale under normal road condition for slope detection. (a) case 1 and (b) case 2.

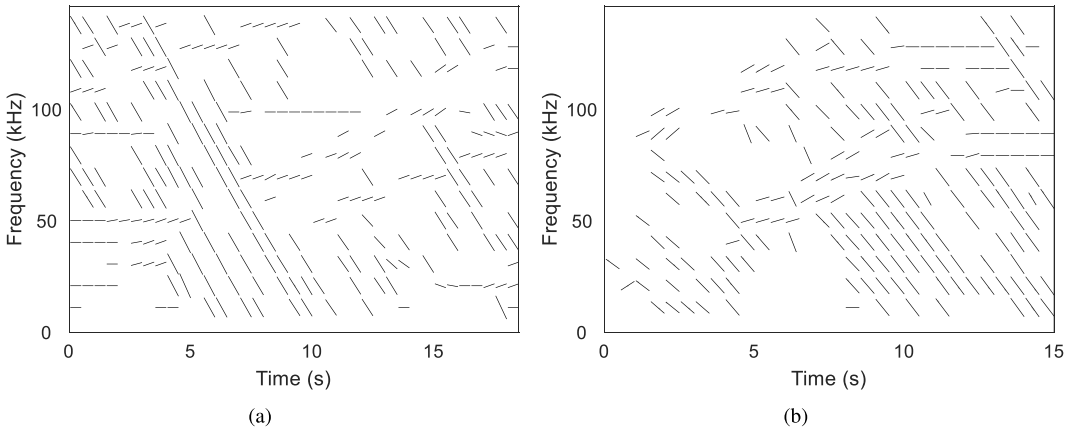

FIGURE 4. Slope map of time-frequency spectrum (slopes are expressed using short tangent segments) using the Hough transform. (a) case 1 and (b) case 2.

To use the Hough transform, the binary spectrum is obtained from the time-frequency spectrum. The time-frequency spectrum is divided into small blocks $P_B(f, m)$ which size is 50 × 10 corresponding to 9.75 kHz × 500 ms, and then it is compared with the threshold Th_{BS} to obtain the binary spectrum of each block $BS(f, m)$:

$$BS(f, m) = \begin{cases} 1, & P_B(f, m) \geq Th_{BS} \\ 0, & P_B(f, m) < Th_{BS} \end{cases} \tag{14}$$

$$Th_{BS} = 0.9 \times \max(P_B(f, m)) \tag{15}$$

The $\max(\cdot)$ represents the maximum value.

The Hough transform is applied to each block of the binary spectrum. The slope is extracted by comparing the Hough transform result of each block $H(\theta, \rho)$ with the threshold Th_{slope}, which is calculated as follows:

$$Th_{slope} = 0.9 \times \max(H(\theta, \rho)) \tag{16}$$

Since $H(\theta, \rho)$ greater than Th_{slope} is extracted, various slope values can be extracted. As most slope values that are extracted are similar to each other, the representative slope of each block is calculated by taking the average. However, when there are slopes of different objects in a block, a few

slopes corresponding to each object are obtained. Therefore, the following process is performed. When a stationary object and a moving object exist at the same time, the representative slope of the corresponding block is obtained by preferential selection of the slope of the stationary object. When there are many moving objects, a moving object having a large number of extracted slopes is selected.

Fig. 4 shows the slope of each block. Comparing Fig. 4(a) with the time-frequency spectrum in Fig. 3(a), it can be seen that the patterns of the stationary and moving objects with large magnitude values in Fig. 3(a) are matched with the slope of each block in Fig. 4(a). The decreasing pattern of the stationary object in Fig. 3(a) has a slope that matches the corresponding block of Fig. 4(a). The moving object also has a similar slope in the block. Fig. 4(b) shows that the slope and frequency band of the block matchs well with the patterns in the time-frequency spectrum of Fig. 3(b).

The slope obtained in Fig. 4 is expressed at a relative velocity $V_r(\theta)$ through (17), which is modified from (10):

$$V_r(\theta) = \frac{slope_\theta \times c \times T}{2B} \tag{17}$$

where, c is the speed of light (3×10^8 m/s); T is the chirp duration; and B is the bandwidth. Using the characteristics of (11), the obtained $V_r(\theta)$ is used as a feature for the classification of the stationary and moving objects through comparison with the velocity of the ego-vehicle. When the feature of the current block is $b(t)$, it is expressed as follows:

$$b(t) = \left| \frac{V_r(\theta) + V_{ego}}{V_{ego}} \right| \tag{18}$$

The feature $b(t)$ is weighted as follows to relate to the previous block:

$$\bar{b}(t) = \alpha b(t) + (1 - \alpha)\bar{b}(t-1) \tag{19}$$

where, $\bar{b}(t)$ is calculated by applying a weight to the values of the current block and the previous block; and α is a weight value that is between 0 and 1.

Fig. 5 and 6 are the slope detection results for case 1 and 2, respectively. Fig. 5(a) and 6(a) show the time-frequency representation in dB scale and the ground-truth of stationary objects are expressed in black dots. To obtain the ground truth, the tagging process was manually carried out by experts. The points in the time-frequency spectrum were tagged with the stationary objects in simultaneously recorded images. Fig. 5(b) and 6(b) show a ground-truth feature map where the black blocks indicate ones where stationary objects exist. Fig. 5(c) and 6(c) is the feature $\bar{b}(t)$ of each block obtained through (19), and the gray scale is a representation of the possibility whether objects are stationary or moving. Fig. 5(d) and 6(d) is a histogram that shows the distribution of the feature of the stationary and moving objects, and the distribution of the histogram is modeled using Gaussian modeling. Fig. 5(d) and 6(d) shows that the stationary object is distributed mainly before 0.4, and the moving object is widely distributed according to the movement. Hence, the proposed feature $\bar{b}(t)$ can discriminate the stationary and moving objects.

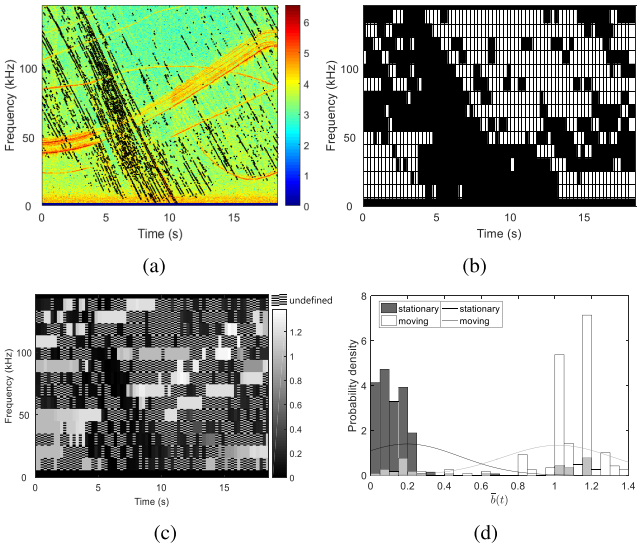

FIGURE 5. Slope detection results of case 1. (a) time-frequency representation of the radar signal in dB scale and ground-truth of stationary objects (black dots), (b) ground-truth feature map, (c) proposed feature($\bar{b}(t)$) map, and (d) histogram that show the distribution of the feature of each object.

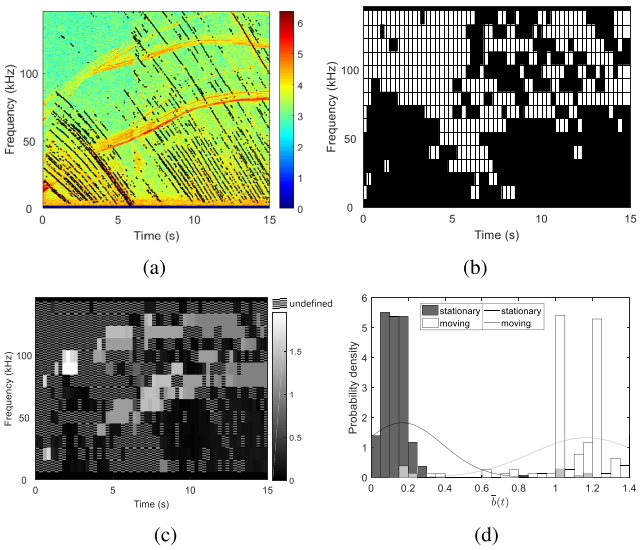

FIGURE 6. Slope detection results of case 2. (a) time-frequency representation of the radar signal in dB scale and ground-truth of stationary objects (black dots), (b) ground-truth feature map, (c) proposed feature($\bar{b}(t)$) map, and (d) histogram that show the distribution of the feature of each object.

V. EXPERIMENTAL RESULTS

In order to verify the validity of the proposed method, we have used a 77 GHz FMCW radar signal measured in the real road environment. The experiments in the real road environment were performed by Mando Corporation (Republic of Korea). The bandwidth (B) of the transmitted signal is 500 MHz, and the chirp duration (T) is 5 ms with the center frequency (f_c)

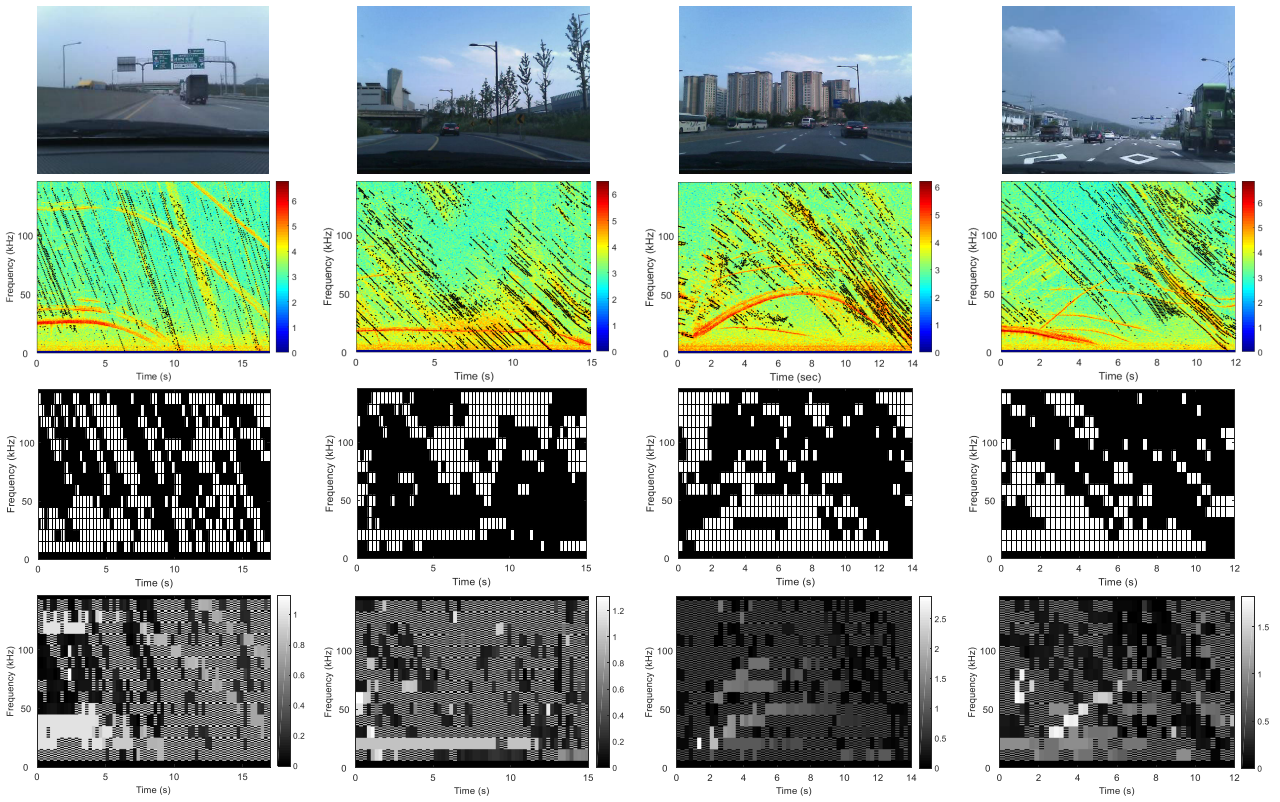

(a)

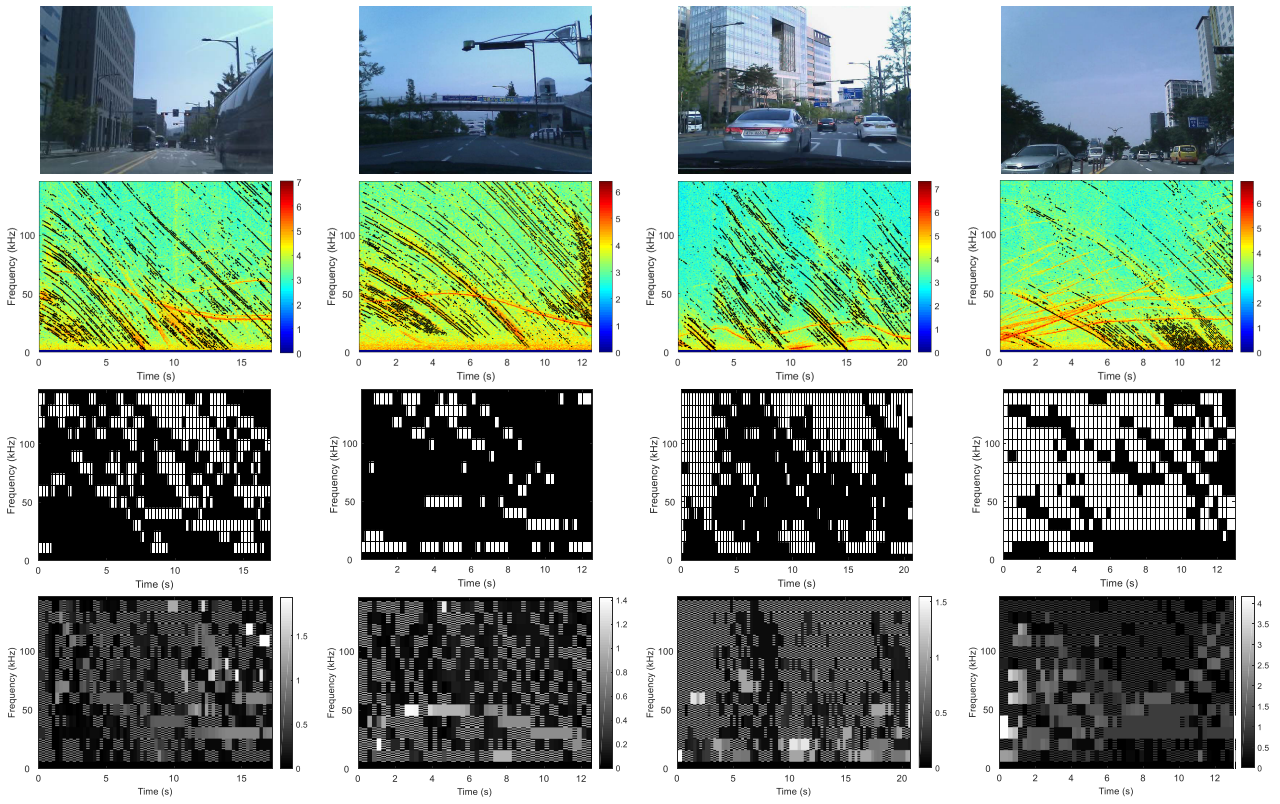

(b)

FIGURE 7. Time-frequency representation in dB scale and slope detection results under expressway and normal road conditions. (a) expressway condition (cases 3-6), and (b) normal road condition (cases 7-10).

TABLE 1. Gaussian modeling for each object and similarity between modeling.

Case	mean ± std		Hellinger distance	KS test
	Stationary	Moving		
1	0.1976±0.2852	1.0179±0.2974	0.7930	0.8410
2	0.1683±0.2183	1.1668±0.3002	0.9167	0.9467
3	0.1480±0.2001	0.8440±0.1946	0.8881	0.9221
4	0.2193±0.2099	0.9074±0.2394	0.8309	0.8747
5	0.1097±0.1214	1.0190±0.4333	0.8604	0.9170
6	0.1237±0.1329	0.9787±0.3440	0.8866	0.9352
7	0.1146±0.1312	0.8224±0.3762	0.8010	0.8598
8	0.1242±0.1786	0.8532±0.2965	0.8549	0.8989
9	0.1598±0.1649	0.8616±0.3380	0.7926	0.8493
10	0.1701±0.3181	1.4073±0.5945	0.7790	0.8351

at 76.5 GHz. The block size of the experimental environment is (50 × 10), and the whole frequency band is divided into 14 sections. A moving window that slides ahead 5 scans at a time is applied, in order to reflect the similarity to the previous block, and α in (19) is 0.9. Fig. 7(a) and (b) show the data under the expressway and normal road condition, respectively. Using the data in Fig. 7, experimental results are presented. In Fig. 7, the first row is the image of the actual driving environment, the second row is the time-frequency spectrum, the third row is the ground-truth feature map, and the last row is the figure that shows the feature $\overline{b}(t)$ of each block. The ground-truth feature map is the result of visually checking whether there is a pattern of a stationary object in each block. It is used for comparison with the feature $\overline{b}(t)$ of each block. As a result, stationary and moving objects are modeled using the statistical properties of the feature $\overline{b}(t)$, and the similarity between modeling is quantified.

Table 1 summarizes the experimental results for each data. The distribution of $\overline{b}(t)$ for stationary and moving objects was represented using Gaussian model. Hellinger distance and KS test were used to quantify the similarity of Gaussian distribution of stationary and moving objects. The Hellinger distance is a type of f-divergence that measures the difference between two probability distributions. f-divergence is an average, weighted by the function f, of the odds ratio given by P and Q. The function $f(t)$ of the Hellinger distnace is $(\sqrt{t}-1)^2$, and the Hellinger distance is expressed as follows:

$$D_H(P,Q) = \frac{1}{\sqrt{2}}\sqrt{\sum_i (\sqrt{P(i)} - \sqrt{Q(i)})^2} \tag{20}$$

where, $P(i)$ and $Q(i)$ are the probability distribution of each sample. The Hellinger distance has a value between 0 and 1, and the farther the distance between the two distributions is, the greater its value becomes.

The KS test is one of the most useful and general non-parametric method for quantifying the distance between two distributions, and is sensitive to differences in both location and shape of the cumulative distribution function. The KS test is calculated as follows using the cumulative distributions $F_1(x)$ and $F_2(x)$. The range of values is between 0 and 1:

$$D_{KS} = \max |F_1(x) - F_2(x)| \tag{21}$$

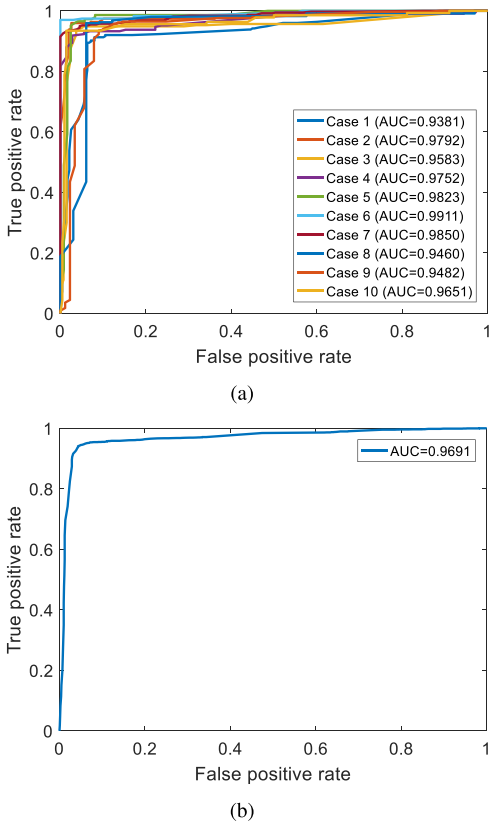

FIGURE 8. ROC curve results. (a) ROC curve for each data, and (b) ROC curve for all data.

The results of Gaussian modeling in Table 1 show that the average of stationary objects is (0.1 to 0.2), and the average of moving objects is (0.8 to 1.1). The Hellinger distance and KS test that quantify the similarity between the two distributions are mainly larger that 0.8. We can observe that the distance between the distribution of stationary and moving objects is far away. Several thresholds were applied to look at the classification performance, and the receiver operating characteristics (ROC) curve was applied to verify the performance. The ROC curve is created by plotting the true positive rate (TPR) against the false positive rate (FPR). TPR, which is also known as sensitivity, is a rate classifying as positive in the actual positive data. FPR is a rate that is erroneously classified as positive in the actual negative data. TPR and FPR are calculated as follows using the true positive (TP), false negative (FN), false positive (FP), and true negative (TN) of the confusion matrix:

$$TPR = \frac{TP}{TP + FN} \tag{22}$$

$$FPR = \frac{FP}{FP + TN} \tag{23}$$

TABLE 2. Correlation coefficients for each datum.

Case	1	2	3	4	5	6	7	8	9	10
Correlation coefficient	0.8155	0.8866	0.8589	0.8109	0.8291	0.8741	0.8127	0.7391	0.8022	0.7684

FPR is the rate of classifying stationary objects among moving objects, and TPR is the rate of classifying stationary objects among stationary objects. The area under the curve (AUC) that represents the area of the ROC graph is an indicator of the performance of the ROC curve. The maximum value of AUC is 1, which means that TPR is high, regardless of FPR. This means that the performance of the classification model is good. Fig. 8(a) shows the ROC curve using the confusion matrix for each of the data in Cases 1–10, while Fig. 8(b) shows the result by combining the confusion matrix of all data.

In Fig. 8, the AUC of each ROC curve is 0.94 or higher, and the AUC of the all data is 0.9691. Therefore, we have verified that the performance of the classification model based on the proposed feature is good.

In addition, the correlation coefficient was calculated to compare the $\bar{b}(t)$ of each block and the ground-truth feature map. When the number of samples is N, the correlation coefficient can be calculated as follows:

$$\rho(A, B) = \frac{1}{N-1} \sum_{i=1}^{N} \left(\frac{A_i - \mu_A}{\sigma_A} \right) \left(\frac{B_i - \mu_B}{\sigma_B} \right) \quad (24)$$

where, A and B represent the ground-truth feature and $\bar{b}(t)$ values in the block, respectively. In the case of the ground-truth feature map, the values is 0 for a stationary object, and 1 for a moving object. μ_A and σ_A are the mean and standard deviation of A, respectively. Table 2 summarizes the correlation coefficient results of each datum. The correlation coefficient between the ground-truth feature and the $\bar{b}(t)$ values of each block mostly shows a value of 0.8 or higher, which shows a strong linear relationship. That is, we can confirm the high similarity between the ground-truth feature map and the proposed feature.

VI. CONCLUSION

In this paper, we have analyzed the time-frequency characteristics of stationary and moving objects, and proposed a method of the discrimination and spectral mapping of stationary and moving objects. A stationary object on the time-frequency spectrum shows a pattern in which the frequency decreases according to the velocity of the ego-vehicle. The slope of the pattern in the time-frequency spectrum was measured using the Hough transform, and the difference between the measured velocity by the slope and the velocity of the ego-vehicle was defined as a feature. The stationary and moving objects were mapped on the time-frequency spectrum using the proposed feature, and the experimental results were verified through the 77 GHz FMCW radar signal measured in real road environment.

In order to verify the performance of the proposed feature, the statistical characteristics of stationary and moving objects were modeled, and the similarity between modeling was quantified. In addition, the classification result according to the threshold was analyzed through the ROC curve. Although the shape or type of stationary objects such as upper structure, guardrail, and road sign is not distinguished, we have classified the stationary and moving objects on the time-frequency spectrum.

REFERENCES

[1] G. Bresson, Z. Alsayed, L. Yu, and S. Glaser, "Simultaneous localization and mapping: A survey of current trends in autonomous driving," *IEEE Trans. Intell. Veh.*, vol. 2, no. 3, pp. 194–220, Sep. 2017.

[2] C. Lundquist, U. Orguner, and T. B. Schon, "Tracking stationary extended objects for road mapping using radar measurements," in *Proc. IEEE Intell. Vehicles Symp.*, Jun. 2009, pp. 405–410.

[3] C. Lundquist, L. Hammarstrand, and F. Gustafsson, "Road intensity based mapping using radar measurements with a probability hypothesis density filter," *IEEE Trans. Signal Process.*, vol. 59, no. 4, pp. 1397–1408, Apr. 2011.

[4] M. Buehler, K. Iagnemma, and S. Singh, "Special issue on the 2007 DARPA urban challenge," *J. Field Robot.*, vol. 25, nos. 8–10, p. 9, 2008.

[5] J. Han, D. Kim, M. Lee, and M. Sunwoo, "Enhanced road boundary and obstacle detection using a downward-looking LIDAR sensor," *IEEE Trans. Veh. Technol.*, vol. 61, no. 3, pp. 971–985, Mar. 2012.

[6] L. Zhou and Z. Deng, "LIDAR and vision-based real-time traffic sign detection and recognition algorithm for intelligent vehicle," in *Proc. 17th Int. IEEE Conf. Intell. Transp. Syst. (ITSC)*, Oct. 2014, pp. 578–583.

[7] E. Coelingh, A. Eidehall, and M. Bengtsson, "Collision warning with full auto brake and pedestrian detection—A practical example of automatic emergency braking," in *Proc. 13th Int. IEEE Conf. Intell. Transp. Syst.*, Sep. 2010, pp. 155–160.

[8] Z. Feng, M. Li, M. Stolz, M. Kunert, and W. Wiesbeck, "Lane detection with a high-resolution automotive radar by introducing a new type of road marking," *IEEE Trans. Intell. Transp. Syst.*, vol. 20, no. 7, pp. 2430–2447, Jul. 2019.

[9] S. Lee, B.-H. Lee, J.-E. Lee, and S.-C. Kim, "Statistical characteristic-based road structure recognition in automotive FMCW radar systems," *IEEE Trans. Intell. Transp. Syst.*, vol. 20, no. 7, pp. 2418–2429, Jul. 2019.

[10] F. Diewald, J. Klappstein, F. Sarholz, J. Dickmann, and K. Dietmayer, "Radar-interference-based bridge identification for collision avoidance systems," in *Proc. IEEE Intell. Vehicles Symp. (IV)*, Jun. 2011, pp. 113–118.

[11] S. Lee, Y.-J. Yoon, J.-E. Lee, and S.-C. Kim, "Human–vehicle classification using feature-based SVM in 77-GHz automotive FMCW radar," *IET Radar, Sonar Navigat.*, vol. 11, no. 10, pp. 1589–1596, Oct. 2017.

[12] E. Schubert, F. Meinl, M. Kunert, and W. Menzel, "High resolution automotive radar measurements of vulnerable road users—Pedestrians & cyclists," in *IEEE MTT-S Int. Microw. Symp. Dig.*, Apr. 2015, pp. 1–4.

[13] A. Carr, L. Cuthbert, and A. Olver, "Digital signal processing for target detection FMCW radar," *IEE Proc. F-Commun. Radar Signal Process.*, vol. 128, no. 5, p. 331, 1981.

[14] J.-E. Lee, H.-S. Lim, S.-H. Jeong, S.-C. Kim, and H.-C. Shin, "Enhanced iron-tunnel recognition for automotive radars," *IEEE Trans. Veh. Technol.*, vol. 65, no. 6, pp. 4412–4418, Jun. 2016.

[15] H.-B. Lee, J.-E. Lee, H.-S. Lim, S.-H. Jeong, and S.-C. Kim, "Clutter suppression method of iron tunnel using cepstral analysis for automotive radars," *IEICE Trans. Commun.*, vol. E100.B, no. 2, pp. 400–406, 2017.
[16] J.-E. Lee, H.-S. Lim, S.-H. Jeong, H.-C. Shin, S.-W. Lee, and S.-C. Kim, "Harmonic clutter recognition and suppression for automotive radar sensors," *Int. J. Distrib. Sensor Netw.*, vol. 13, no. 9, Sep. 2017, Art. no. 155014771772979.
[17] R. O. Duda and P. E. Hart, "Use of the Hough transformation to detect lines and curves in pictures," *Commun. ACM*, vol. 15, no. 1, pp. 11–15, Jan. 1972.
[18] L. Le Cam, and G. L. Yang, *Asymptotics in Statistics: Some Basic Concepts*. Berlin, Germany: Springer, 2000, pp. 42–48.
[19] F. J. Massey, "The Kolmogorov-Smirnov test for goodness of fit," *J. Amer. Stat. Assoc.*, vol. 46, no. 253, pp. 68–78, Mar. 1951.
[20] T. Fawcett, "An introduction to ROC analysis," *Pattern Recognit. Lett.*, vol. 27, no. 8, pp. 861–874, Jun. 2006.
[21] J. L. Rodgers and W. A. Nicewander, "Thirteen ways to look at the correlation coefficient," *Amer. Statistician*, vol. 42, no. 1, p. 59, Feb. 1988.
[22] A. Stove, "Linear FMCW radar techniques," *IEE Proc. F (Radar Signal Process.)*, vol. 139, no. 5, p. 343, Oct. 1992.
[23] H. Song, S. Cho, K.-J. You, and H.-C. Shin, "Improving DOA estimation and preventing target split using automotive radar sensor arrays," *IEICE Trans. Fundamentals*, vol. E101.A, no. 3, pp. 590–594, 2018.

HEEMANG SONG received the B.S. degree in electronic engineering from Soongsil University, Seoul, South Korea, in 2015, where he is currently pursuing the Ph.D. degree. Since 2015, he has been a Research Assistant with the Department of Electronic Engineering, Soongsil University. His research interest includes radar signal processing focusing on automobile.

HYUN-CHOOL SHIN (Member, IEEE) received the Ph.D. degree in electronic and electrical engineering from the Pohang University of Science and Technology (POSTECH), South Korea, in 2004. From 2004 to 2007, he was a Postdoctoral Researcher with the Department of Biomedical Engineering, School of Medicine, Johns Hopkins University. Since 2007, he has been a Professor of electronic engineering with Soongsil University. His research interests include intelligent signal processing focusing on neural system and automotive radar.